Circuits Syst Signal Process
DOI 10.1007/s00034-014-9844-z

A Robust Demodulator for OQPSK–DSSS System

Shengchen Dai · Hua Qian · Kai Kang · Weidong Xiang

Received: 15 December 2013 / Revised: 13 June 2014 / Accepted: 16 June 2014

Abstract IEEE802.15.4 standard has quickly become a benchmark in the era of Internet of things. The mandatory mode of 2.4 GHz physical layer of IEEE802.15.4 standard employs offset quadrature phase shift keying (OQPSK) modulation with direct sequence spread spectrum (DSSS). The performance of conventional differential demodulator is not satisfactory. The coherent demodulator is vulnerable to initial phase mismatch or frequency offset. In this paper, we propose a new non-coherent demodulator for the OQPSK–DSSS system. The proposed demodulator is robust against initial phase mismatch and frequency offset. At −1.3 dB SNR in additive white Gaussian noise channel, the proposed demodulator achieves the target sensitivity at 1 % packet error rate. Simulation results demonstrate the effectiveness and robustness of the proposed demodulator.

S. Dai · H. Qian (✉) · K. Kang
Shanghai Institute of Microsystem and Information Technology (SIMIT), Chinese Academy of Sciences (CAS), Shanghai 200050, China
e-mail: hua.qian@shrcwc.org

S. Dai · H. Qian · K. Kang
Shanghai Research Center for Wireless Communications, Shanghai 200335, China
e-mail: shengchen.dai@shrcwc.org

S. Dai · H. Qian · K. Kang
Key Laboratory of Wireless Sensor Network and Communication, SIMIT, CAS, Shanghai 200050, China
e-mail: kai.kang@shrcwc.org

W. Xiang
Electrical and Computer Engineering Department, University of Michigan, Dearborn, Dearborn 48128, MI, USA
e-mail: xwd@umd.umich.edu

Published online: 04 July 2014

Keywords IEEE802.15.4 · OQPSK · DSSS · Non-coherent demodulation · Frequency offset · Phase mismatch

1 Introduction

IEEE802.15.4 standard is developed to meet the needs for simple, low-power and low-cost wireless communications [7]. In 2.4 GHz physical layer (PHY) of IEEE802.15.4, direct sequence spread spectrum (DSSS) is applied to improve system performance in noisy environments. The transmitter modulates the carrier using offset quadrature phase shift keying (OQPSK) with half-sine pulse shaping filter. This modulation is identical to minimum shift keying (MSK) [2]. Since MSK exhibits a constant signal envelope, the transmitter can be power efficient by utilizing nonlinear power amplifiers.

At the receive side, the required SNR of the coherent demodulator is −2.3 dB to achieve the target sensitivity [8]. However, this demodulator is sensitive to initial phase mismatch and residual carrier frequency offset. The computational overhead for accurate initial phase mismatch and frequency offset estimation and compensation is not acceptable for low-cost and low-power design. The conventional MSK differential demodulator, on the other hand, is simple to implement. However, its performance is not satisfactory. The SNR requirement of differential demodulation scheme proposed in Wang and Huang [15] is 9.0 dB at the sensitivity level. The demodulator with phase-axis crossing detector (PACD) algorithm is proposed in Yu et al. [17]. The SNR requirement is 8.8 dB. Differential demodulator with sine phase comparator achieves 8.4 dB [16]. The asynchronous zero crossing detector (AZCD) algorithm is used for demodulation in Ghazi et al. [3] and non-coherent energy detection (ED) demodulator is implemented in Kreiser and Olonbayar [5]. Demodulator for orthogonal modulation is proposed in Park et al. [12], which is robust against large frequency offset. Differential detection and cross-correlation are applied in Yin et al. [18]. The SNR requirement at the sensitivity level is 2.9 dB. The performance of the existing non-coherent demodulators is all not satisfactory. The gap between the differential demodulators and the coherent demodulator is at least 5.2 dB.

In this paper, we propose a non-coherent demodulator for OQPSK–DSSS system, which is robust against initial phase mismatch and frequency offset in additive white Gaussian noise (AWGN) and Rayleigh fading channels. The SNR requirement at the sensitivity level is −1.3 dB in AWGN channel. The complexity of the proposed demodulator is lower than that of the coherent demodulator. The performance of the proposed demodulator is 4.2 dB better than that of differential demodulator in Yin et al. [18]. We also demonstrate the effectiveness and robustness of the proposed demodulator against the coherent demodulator.

The rest of this paper is organized as follows: In Sect. 2, we introduce the system setup of the IEEE802.15.4 transceiver. In Sect. 3, we briefly go over the coherent demodulator and derive the proposed demodulator. An example is given to illustrate the detection process. We analyzes the robustness of the proposed non-coherent demodulator in Sect. 4. In Sect. 5, simulation results validate advantages of the proposed demodulator. Section 6 concludes the paper.

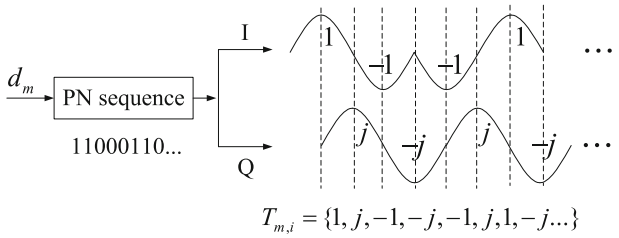

Fig. 1 Modulation scheme of the OQPSK–DSSS system

2 System Setup

In 2.4 GHz PHY design of IEEE802.15.4 standard, information bits are spread into chips with DSSS. In the bit-to-symbol block, every four bits are mapped into one data symbol, which is represented as d_m, where m is the symbol index. The data symbol d_m is then converted to a 32 chip pseudo-noise (PN) sequence [4], which is denoted by $T_{m,i}$, where m is the symbol index and i is the chip index in a symbol. The OQPSK modulation with half-sine pulse shaping filter is applied in chip level. The PN sequence is separated as I-branch and Q-branch shown in Fig. 1. In I-branch, if the chip value of PN sequence is 0, $T_{m,i}$ is modulated to -1, otherwise it remains 1. In a similar way, if the chip value is 0 in Q-branch, $T_{m,i}$ is modulated to $-j$, otherwise it changes to j.

Let us define $s_{l,i}$ as the ith chip in lth data symbol of the transmitted chip level signal. When the transmitted data symbol is d_m, $s_{l,i}$ is mapped to $T_{m,i}$. The complex envelop of the transmitted signal can be represented as

$$s(t) = \sum_{l=0}^{L-1} \sum_{i=0}^{31} s_{l,i} g(t - iT_c - 32lT_c), \tag{1}$$

where L is the number of transmitted data symbols, T_c is the chip interval, and $g(t)$ is the half-sine pulse shaping filter, which can be described as

$$g(t) = \begin{cases} \sin(\pi t/2T_c), & 0 \le t \le 2T_c, \\ 0, & \text{otherwise.} \end{cases} \tag{2}$$

In short-range communications such as IEEE802.15.4, the effects of channel fading would not be predominant. AWGN channel is widely utilized for the development and analysis of demodulators. In real systems, the propagation delay, the digital sampling mismatch and timing synchronization error lead to initial phase mismatch. The low-cost local oscillators used in transmitter and receiver results in frequency offset and frequency drift. Considering these imperfections, the received analog baseband signal can be represented as

$$r(t) = \mathrm{e}^{j(2\pi f t + \theta)} s(t) + n(t), \tag{3}$$

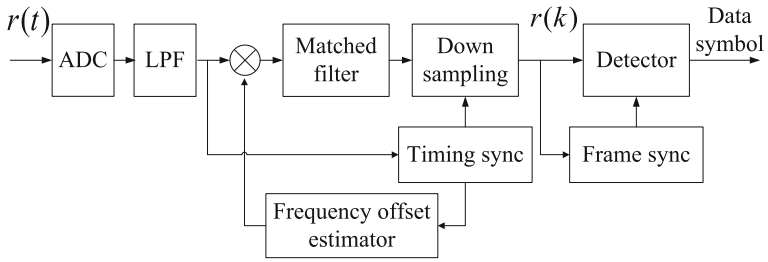

Fig. 2 Block diagram of the proposed demodulator

where f is the frequency offset between the transmitter and the receiver, and θ is the initial phase mismatch at the receiver side. We assume that θ is an unknown random variable that is uniformly distributed in $[-\pi, \pi)$, and $n(t)$ is the baseband equivalent AWGN noise of the system. The initial phase mismatch, frequency offset and additive noise are assumed to be statistically independent of each other.

3 The Proposed Non-coherent Demodulator

In this section, we introduce a robust demodulator to IEEE802.15.4 OQPSK–DSSS signal based on a non-coherent detector, which does not require the prior knowledge of the initial phase mismatch and frequency offset of the received sequence. The block diagram of the proposed demodulator is shown in Fig. 2.

In Fig. 2, a direct down conversion architecture is used. A low intermediate frequency (IF) architecture is also applicable with an additional digital mixer that moves the low IF signal to baseband. Incoming baseband analog signal $r(t)$ is first sampled by the analog-to-digital converter (ADC). In order to remove inter-channel interference and out-of-band noise, a low-pass filter (LPF) is inserted after the ADC block. Preamble of a packet can be used for automatic gain control (AGC), timing synchronization and frequency offset estimation. Frequency offset estimation and compensation are performed after timing synchronization. In order to maximize the SNR of the received signal, a matched filter is applied. The coefficients of the matched filter are sampling values of (2) since the original pulse shaping filter is symmetrical. After down sampling, the received chip level signal $r(k)$ is obtained. Symbol boundary is determined by frame synchronization. With perfect synchronization, the received chip level signal before frequency offset compensation can be represented as

$$r(k) = \sum_{l=0}^{L-1} \sum_{i=0}^{31} r_{l,i}\,\delta(k - i - 32l), \tag{4}$$

where $\delta(k)$ is the unit impulse function and $r_{l,i}$ is the ith chip of lth symbol with initial phase mismatch and frequency offset in receiver. The soft chip $r_{l,i}$ can be represented as

$$r_{l,i} = \mathrm{e}^{j(2\pi f i T_c + \theta)} s_{l,i} + n_i, \tag{5}$$

where $n_i = n_{i,c} + jn_{i,s}$, is AWGN noise with the variance of σ^2. Given $s_{l,i}$, $r_{l,i}$ is also a complex Gaussian distributed random variable. With correct chip boundary, $r(k)$ can be decoded into symbols for every 32 soft chips.

3.1 Frequency Offset Estimation

The low-cost local oscillators used in transmitter and receiver may have different frequency offset and frequency drift characteristics. The preamble of the IEEE802.15.4 can be applied to perform the frequency offset estimation [1,9]. For the frequency offset estimation, $s_{l,i}$ is known in prior. The input chips for frequency offset estimator can be described as

$$z_{l,i} = r_{l,i}s_{l,i} = \mathrm{e}^{j(2\pi f i T_c + \theta)} + v_i, \tag{6}$$

where $v_i = n_i s_{l,i}$, and v_i is a zero mean Gaussian random distribution sequence that is independent of f and θ. A robust frequency offset estimator is given by [6]:

$$\hat{f} = \frac{1}{2\pi T_c N} \arg \sum_{i=0}^{N-1} \left(z_{l,i}^* z_{l,i+1}\right), \tag{7}$$

where N is the observation sequence length and "*" is conjugate operation.

The performance of the frequency estimator can be improved when the product $(z_{l,i}^* z_{l,i+1})$ is replaced by $(z_{l,i}^* z_{l,i+D})$ [10]. The simplified Kay D-spaced (SKD) estimator is

$$\hat{f} = \frac{1}{2\pi T_c N} \arg \sum_{i=0}^{N-1} \left(z_{l,i}^* z_{l,i+D}\right). \tag{8}$$

Therefore, the key is to estimate a virtual frequency offset Df. The value D must be a positive integer and meet the condition of $2\pi D f T_c < \pi$. Denote Δf the residual frequency offset after compensation. The variance of Δf is given by

$$\mathrm{var}(\Delta f) = \frac{1}{(2\pi T_c D)^2}\left(\frac{D}{N^2(E_b/N_0)} + \frac{1}{2N(E_b/N_0)^2}\right). \tag{9}$$

CRLB is used to measure the performance of estimators for frequency offset estimation. For the frequency offset estimator, the variance of CRLB [14] is

$$\mathrm{var}(\Delta f) = \frac{3}{2\pi^2 E_b/N_0 T_c^2 N(N^2-1)}. \tag{10}$$

In 2.4 GHz PHY of IEEE802.15.4, the preamble is mapped into 8 fixed PN sequences corresponding to symbol index "**0**." There are 256 known chips in preamble. The sequence length N for frequency offset estimators equals to 256. According to IEEE802.15.4 standard, the maximum frequency offset is ±200 kHz. D must to be

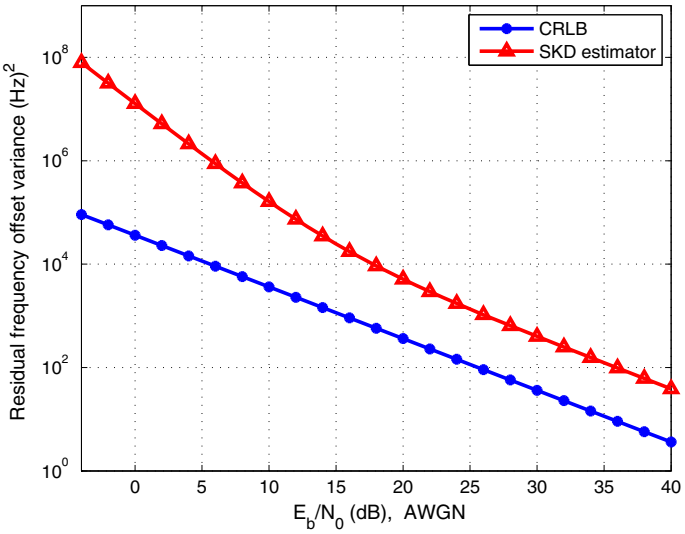

Fig. 3 Performance of SKD estimator for IEEE802.15.4 signals in AWGN channel and CRLB. The differential space of SKD estimator is $D = 4$

an even integer due to OQPSK modulation with half-sine pulse shaping filter. In order to meet the condition $2\pi DfT_c < \pi$, D equals to 4 in SKD estimator.

Figure 3 shows the variances of the residual frequency offsets given by SKD estimator and CRLB. There exists a significant gap in terms of the residual frequency offsets between SKD estimator and CRLB. More sophisticated frequency offset estimator can help to reduce the gap. However, the CRLB still serves as a lower bound for all data-aided frequency offset estimator.

3.2 Detection Scheme

The signal for detection after synchronization and frequency offset compensation can be described as

$$r_{l,i} = \mathrm{e}^{j(2\pi \Delta f i T_c + \Delta\theta)} s_{l,i} + n_i, \tag{11}$$

where Δf is the residual frequency offset at the receiver side. $\Delta\theta$ is the residual phase error. Frequency offset insensitive detection for orthogonal modulation using decision-aided ML detection is derived in Park and Park [13]. It is an improved differential ML detection algorithm. However, the differential detection algorithm degrades the performance. In this section, we propose a new non-coherent detection algorithm, which is not based on differential detection. The proposed method, which costs low computation, greatly improves the performance.

Detector is inserted after the frequency offset compensation. The coherent detector can be used for OQPSK–DSSS demodulators without residual phase error and residual frequency offset. At the ideal sampling time, the ith chip of lth symbol in the received

chip level signal is $r_{l,i}$. Since there exists no residual phase error and residual frequency offset, the real part of $r_{l,i}$ carries the whole chip information in I-branch. The imaginary part of $r_{l,i}$ is the chip information in Q-branch.

The soft information chips in lth symbol for the coherent detector can be described as

$$r'_{l,i} = \begin{cases} Re\{r_{l,i}\}, & (i \bmod 2) = 0, \\ j \times Im\{r_{l,i}\}, & \text{otherwise}, \end{cases} \tag{12}$$

where $Re\{r_{l,i}\}$ is the real part of $r_{l,i}$, and $Im\{r_{l,i}\}$ is the imaginary part of $r_{l,i}$. Since the variable $r_{l,i}$ is a complex Gaussian-distributed random variable, we conclude that $r'_{l,i}$, which is the real or imaginary part of $r_{l,i}$, is a Gaussian-distributed random variable with the variance of $\sigma^2/2$. In this case, the noise in one branch is completely ignored when detection is made on the other branch.

For the coherent demodulator, we consider the conditional probability density function (PDF) of the received signal given a prior knowledge of the transmitted symbol index m:

$$f\left(\boldsymbol{r}'_{\boldsymbol{l}}|m\right) = \prod_{i=0}^{31} \frac{1}{\pi} \mathrm{e}^{-|r'_{l,i}-s_{l,i}|^2} = \left(\frac{1}{\pi}\right)^{31} \prod_{i=0}^{31} \mathrm{e}^{-\left(|r'_{l,i}|^2+1\right)} \times \mathrm{e}^{2\sum_{i=0}^{31}\left(r'_{l,i}\right)^* s_{l,i}}, \tag{13}$$

where $\boldsymbol{r}'_{\boldsymbol{l}} = (r'_{l,0}, r'_{l,1}, \ldots, r'_{l,31})$ is the vector of received soft chips in a symbol. Since $\prod_{i=0}^{31} \mathrm{e}^{-(|r'_{l,i}|^2+1)}$ is a constant for all possible m, $\sum_{i=0}^{31} (r'_{l,i})^* s_{l,i}$ is real, and e^x is a monotonically increasing function when x is real, the maximum likelihood (ML) estimator is

$$\hat{m} = \arg\max f\left(\boldsymbol{r}'_{\boldsymbol{l}}|m\right) = \arg\max \sum_{i=0}^{31} \left(r'_{l,i}\right)^* s_{l,i}. \tag{14}$$

Figure 4 shows the top structure of the ML estimator. The "correlation calculator" can be replaced by other correlation calculators. $V_{l,m}$ is the correlation value of the lth received sequence and the local PN sequence corresponding to symbol index m. m varies from 0 to 15. The comparator treats $\hat{m}$ as the transmitted symbol and can be defined as

$$\hat{m} = \arg \max_{m \in [0,15]} V(l, m). \tag{15}$$

The coherent detector structure of (14) is shown in Fig. 4, where the "correlation calculator" is replaced by "coherent correlation calculator." Figure 5 shows the block diagram of the coherent correlation calculator. The inputs $r_{l,i}$ and $T_{m,i}$ are divided into two parts, the real part and the imaginary part. In order to calculate $V_{m,l}$, the accumulators need to be reset at the beginning of every symbol.

In real systems, timing synchronization error leads to residual phase error. The performance of the coherent detector degrades greatly in this case. If the residual phase error is not available, the I-branch and Q-branch of the received soft chip $r_{l,i}$ can not be decoupled. $r_{l,i}$ with residual phase error is used directly to derive the new non-coherent detector. The conditional PDF of the received signal was given a prior knowledge of the transmitted symbol m with residual phase error $\Delta\theta$ is given by

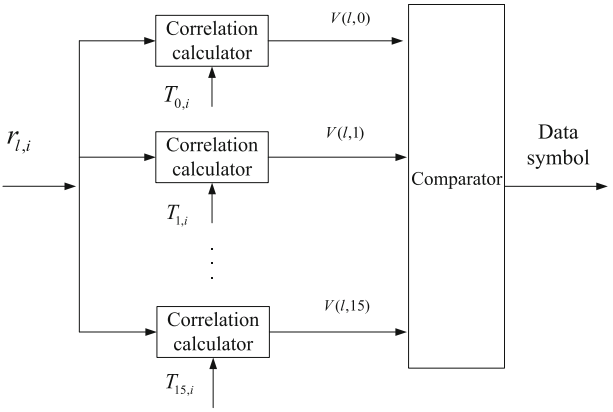

Fig. 4 Top structure of ML detector. The coherent detector and the proposed detector share the same top structure, but they are with different correlation calculator. Sixteen correlation calculators calculate correlation values $V_{l,m}$ between the received baseband chip level signal $r_{l,i}$ and the 16 local PN sequences. m is the index number of PN sequences. The comparator maximizes $V_{l,m}$ when m varies from 0 to 15

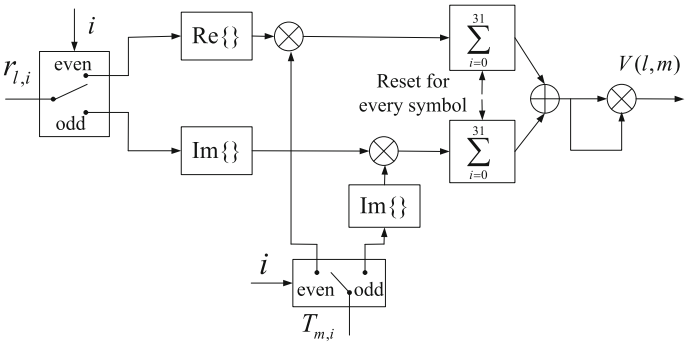

Fig. 5 Block diagram of the coherent correlation calculator

$$f(\boldsymbol{r_l}|, \Delta\theta) = \prod_{i=0}^{31} \frac{1}{\pi} \mathrm{e}^{-|r_{l,i} - e^{j\Delta\theta} s_{l,i}|^2}, \tag{16}$$

where $\boldsymbol{r_l} = (r_{l,0}, r_{l,1}, r_{l,2}, \ldots, r_{l,31})$.

We assume that $\Delta\theta$ is uniformly distributed over $[-\pi, \pi)$. Consequently, the ML estimator is defined as

$$\begin{aligned} \hat{m} &= \arg\max f(\boldsymbol{r_l}|m) = \arg\max \int_{-\pi}^{\pi} f(\boldsymbol{r_l}|m, \Delta\theta) \frac{1}{2\pi} \mathrm{d}\Delta\theta \\ &= \arg\max \left(\frac{1}{\pi}\right)^{32} \prod_{i=0}^{31} \mathrm{e}^{-(|r_{l,i}|^2+1)} \times I_0\left(2\left|\sum_{i=0}^{31} (r_{l,i})^* s_{l,i}\right|\right), \end{aligned} \tag{17}$$

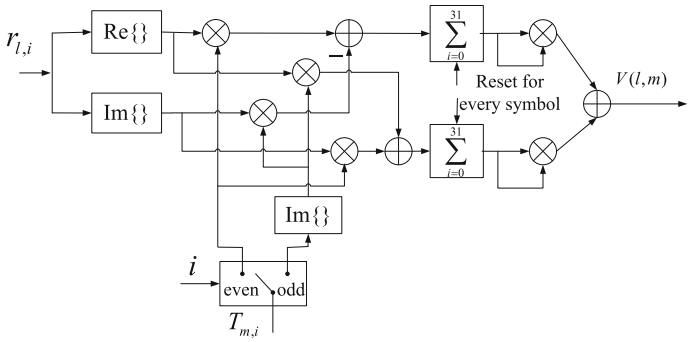

Fig. 6 Block diagram of the proposed correlation calculator

where $I_0(x) = (1/2\pi)\int_{-\pi}^{\pi} \mathrm{e}^{x\cos\Delta\theta}\mathrm{d}\Delta\theta$ is the zeroth-order modified Bessel function of first kind [11]. In (17), $\prod_{i=0}^{31}\mathrm{e}^{-(|r_{l,i}|^2+1)}$ is a constant for all possible m. In addition, $I_0(x)$ is an monotonically increasing function where x is real. The ML estimator in (17) can be simplified as

$$\hat{m} = \arg\max \left| \sum_{i=0}^{31} (r_{l,i})^* s_{l,i} \right|, \tag{18}$$

where $|\cdot|$ means taking modulus of a complex number. The top structure of (18) is the same as the coherent detector in (14). However, the correlation calculator is different. The correlation calculator in Fig. 4 is replaced by the proposed correlation calculator shown in Fig. 6. The coherent detector separates soft chips in I-branch and Q-branch. The soft chip in one branch has no influence on the other branch. Compared to the coherent detector, the proposed detector uses the soft chips with influence from the other branch for decision. The correlation values between soft chips and local PN sequences are calculated. Then, we take the modulus of these correlation values for comparison. This technique leads to the robustness and effectiveness of proposed detector.

An illustrative example shown in Table 1 is applied to describe the process of the proposed detection scheme. In this example, the original transmitted sequence is $\{0, 0, 0, 0\}$. The symbol index m is 0. The corresponding chip index i and the mapped chip value $T_{m,i}$ is shown in the first column and the second column of Table 1. The received soft chip after matched filter $r_{l,i}$ of the proposed detector is shown in the third column. For the coherent detector, the chip for detector $r'_{l,i}$ is shown in the forth column. The signal passes through an AWGN channel with SNR $= -2$ dB, when the residual phase error is -0.3π.

Figure 7 shows the amplitude of the cross-correlation values for the coherent detector in (14) and the proposed detector in (18). From Fig. 7, we observe that the propose detector obtains the maximum amplitude of the cross-correlation value at symbol "**0**," or at the information bits $\{0, 0, 0, 0\}$. However, the coherent detector considers sym-

Table 1 An example of different detectors with SNR $= -2$ dB, when the residual phase error is -0.3π

Chip index	$T_{m,i}$	Proposed soft chip $r_{l,i}$	Coherent soft chip $r'_{l,i}$
0	1	$0.330 + 0.171j$	0.330
1	j	$-0.124 - 0.149j$	$-0.149j$
2	-1	$-0.319 - 0.222j$	-0.319
3	j	$-0.483 - 0.086j$	$-0.086j$
…	…	…	…
28	1	$0.251 - 0.022j$	0.251
29	j	$-0.004 + 0.223j$	$0.223j$
30	1	$0.175 + 0.212j$	0.175
31	$-j$	$0.375 - 0.135j$	$-0.135j$

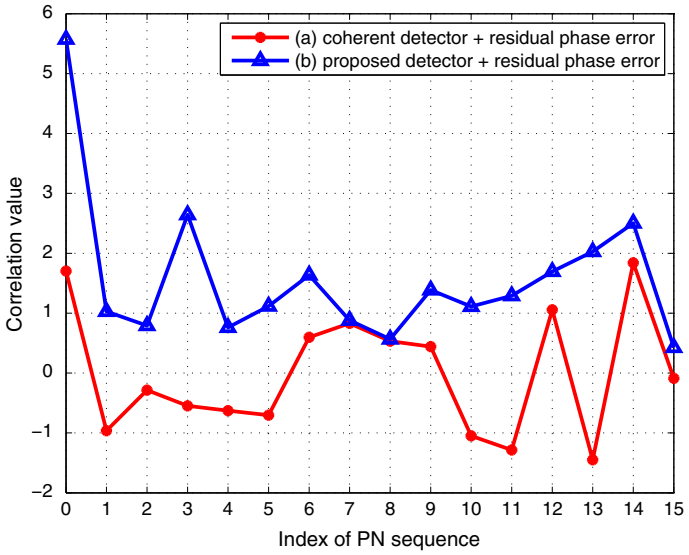

Fig. 7 Correlation values of the proposed detector and the coherent detector in the example. The proposed detector obtains the maximum amplitude of the cross-correlation value at symbol "**0**," or at the information bits {0, 0, 0, 0}. However, the coherent detector treats symbol "**14**" as the transmitted symbol. The proposed detector is robust against residual phase error

bol "**14**" as the transmitted symbol. The propose detector is non-coherent; however, the performance of the coherent detector degrades greatly with residual phase error.

4 Performance Analysis

The proposed demodulator shown in Fig. 2 is robust against initial phase mismatch and frequency offset, which is based on a non-coherent detector. In this section, comparison is made between the proposed detector and the coherent detector. Meanwhile, we analyze the robustness of the proposed demodulator.

The correlation value $V_c(l,m)$ of the coherent detector without initial phase mismatch and frequency offset can be defined as

$$V_c(l,m) = \left\{ \sum_{i=0}^{15} T_{m,2i} Re(r_{l,2i}) - jT_{m,2i+1} Im(r_{l,2i+1}) \right\}^2 = \left\{ \sum_{i=0}^{31} C_{m,i} \right\}^2, \tag{19}$$

where $r_{l,i}$ can be replaced by $s_{l,i} + n_i$ when initial phase mismatch and frequency offset are not considered, and $C_{m,i}$ can be defined as

$$C_{m,i} = \begin{cases} T_{m,i}(Re(s_{l,i}) + n_{i,c}), & (i \bmod 2) = 0, \\ -jT_{m,i}(Im(s_{l,i}) + n_{i,s}), & \text{otherwise.} \end{cases} \tag{20}$$

According to the detection scheme shown in Fig. 6, the correlation value $V_p(l,m)$ of the proposed detector without initial phase mismatch and frequency offset can be defined as

$$V_p(l,m) = \left| \sum_{i=0}^{31} (r_{l,i})^* T_{m,i} \right| = \left| \sqrt{V_c(l,m)} + j \sum_{i=0}^{31} n_{i,1} \right| = V_c(l,m) + \left(\sum_{i=0}^{31} n_{i,1} \right)^2, \tag{21}$$

where $n_{i,1}$ is the zero mean Gaussian random value with the variance of $\sigma^2/2$, which can be represent as

$$n_{i,1} = \begin{cases} -n_{i,s} T_{m,i}, & (i \bmod 2) = 0, \\ -jn_{i,c} T_{m,i}, & \text{otherwise.} \end{cases} \tag{22}$$

Comparing to the coherent detector, the noise term $(\sum_{i=0}^{31} n_{i,1})^2$ in (21) causes performance loss of the proposed detector, when there is no initial phase mismatch or frequency offset. In order to further analyze, we assume that the initial phase mismatch is randomly distributed in $[-\pi, \pi)$, and the impact of residual frequency offset is a Gaussian-distributed residual phase error with zero mean and σ^2 variance in chip level after frequency offset compensation. The initial phase mismatch can be treated as a constant $\bar{\theta}$ in a symbol duration. The total phase error θ_i in ith chip of a symbol is a normally distributed variable with $\bar{\theta}$ mean and σ^2 variance.

The correlation value of the proposed detector with initial phase mismatch and residual frequency offset can be defined as

$$V_\theta(l,m) = \left| \sum_{i=0}^{31} (r_{l,i})^* T_{m,i} \right| = \sum_{p=0}^{31} \sum_{q=0}^{31} C_{m,p} C_{m,q} \cos(\theta_p - \theta_q) + \left(\sum_{i=0}^{31} n_{i,1} \right)^2. \tag{23}$$

We denote $\Delta\theta$ as $\theta_p - \theta_q$, and $\Delta\theta$ is a random Gaussian variable with zero mean and $2\sigma^2$ variance. It is fair to make the following approximation:

$$\cos \Delta\theta \approx 1 - \frac{1}{2}(\Delta\theta)^2. \tag{24}$$

Then, $V_\theta(l,m)$ can be rewritten as

$$V_\theta(l,m) = V_p(l,m) + E, \tag{25}$$

where $V_p(l,m)$ is the correlation value of the proposed correlation calculator without initial phase mismatch and residual frequency offset, and E is given by

$$E = \begin{cases} -\frac{1}{2} \sum_{p=0}^{31} \sum_{q=0}^{31} \{C_{m,p} C_{m,q} (\Delta\theta)^2\}, & p \neq q, \\ 0, & p = q. \end{cases} \tag{26}$$

The distribution of $(\Delta\theta)^2$ is represented as

$$P(u) = \frac{K_0(\frac{|u|}{2\sigma^2})}{2\pi\sigma^2}, \tag{27}$$

where $K_0(x)$ is a modified Bessel function of the second kind. The impact factor E is insignificant when the distribution of $(\Delta\theta)^2$ in (27) is considered. In other words, the proposed detector is robust against initial phase mismatch and residual frequency offset. Comparing to the coherent detector, the performance of the proposed detector is significantly improved with a conventional low-complexity SKD frequency offset estimator.

5 Simulation Results

In this section, we explore the performance of the proposed demodulator and validate the advantage of the proposed demodulator by simulations. The simulation parameters are shown in Table 2. According to the IEEE802.15.4 specification, receiver sensitivity is defined as the threshold input signal power that yields a specified PER = 1 %. The

Table 2 Simulation parameters

Modulation	OQPSK–DSSS
Data rate	250 kbps
Pulse shaping filter	half-sine
Chip rate	2 MChip/s
Payload length	20 bytes
Packet number	10^6

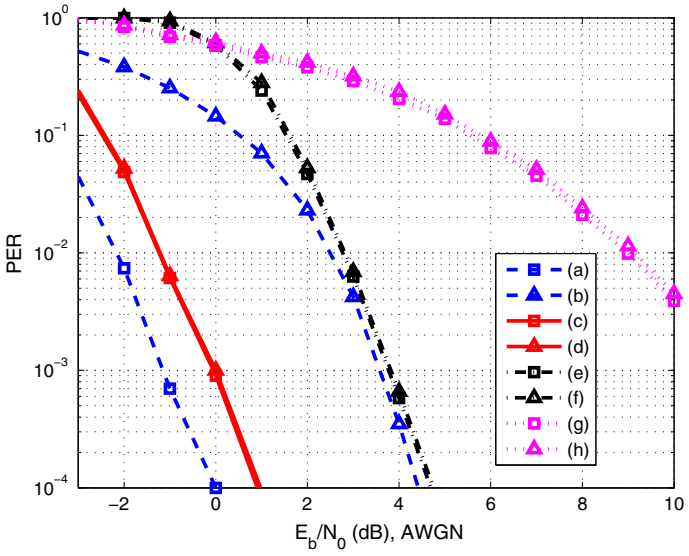

Fig. 8 Performance of detectors with residual phase error and residual frequency offset in AWGN channel. The residual phase error is uniformly distributed in $[-0.25\pi, 0.25\pi)$. The residual frequency offset is Gaussian distributed with zero mean and a variance of CRLB. *Lines* (*a*), (*c*), (*e*) and (*g*) show the PER performance without residual phase error and residual frequency offset of the coherent detector, the proposed detector, the differential detector in Yin et al. [18] and the conventional MSK differential detector, respectively. *Lines* (*b*), (*d*), (*f*) and (*h*) show the PER performance with added residual phase error and residual frequency offset of the coherent detector, the proposed detector, the differential detector in Yin et al. [18] and the conventional MSK differential detector, respectively

setup of PER simulations follow the specification in [4]. For every simulation, the packet number is 10^6.

In the first simulation, we compare PER performance among the proposed detector, the coherent detector, the differential detector in Yin et al. [18] and the conventional MSK differential detector. Residual phase error $\Delta\theta$ caused by imperfection of timing synchronization is set to be a random variable, which is uniformly distributed in $[-0.25\pi, 0.25\pi)$. The residual frequency offset Δf is random Gaussian distributed with zero mean and a variance of CRLB. Figure 8 shows the PER performance of different cases. Lines (a), (c), (e) and (g) show the PER performance without residual phase error and residual frequency offset of the coherent detector, the proposed detector, the differential detector in Yin et al. [18] and the conventional MSK dif-

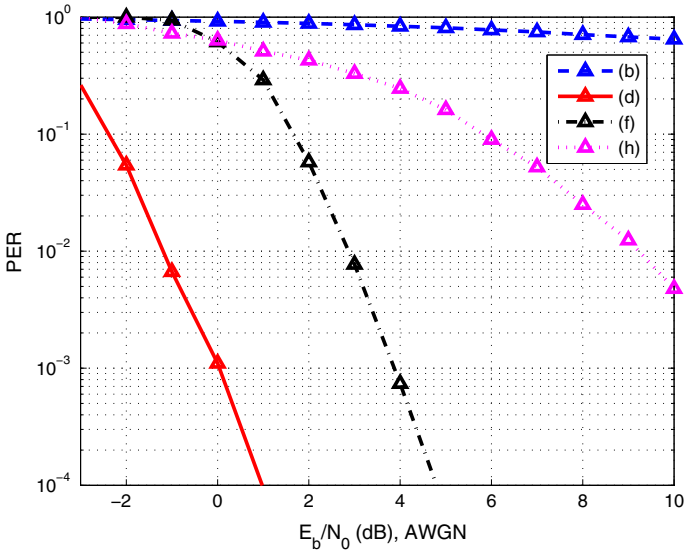

Fig. 9 Performance of demodulators in a real system with AWGN channel. The initial phase mismatch is uniformly distributed in $[-\pi, \pi)$ and the frequency offset is uniformly distributed in [−200 kHz, 200 kHz). The initial phase mismatch is estimated and compensated in timing sync block. The frequency offset is estimated with the SKD estimator in frequency offset estimator block. *Lines* (*b*), (*d*), (*f*) and (*h*) show the PER performance of a demodulation system with initial phase mismatch and frequency offset of the coherent detector, the proposed detector, the differential detector in Yin et al. [18] and the conventional MSK differential detector, respectively

ferential detector, respectively. Lines (b), (d), (f) and (h) show the PER performance with added residual phase error and residual frequency offset of the coherent detector, the proposed detector, the differential detector in Yin et al. [18] and the conventional MSK differential detector, respectively. From the simulation, we observe that with no impairments, the coherent detector achieves the sensitivity at SNR = −2.3 dB. However, its performance degrades to SNR = 2.5 dB with random impairments inserted in the simulation, which are typical and inevitable in a practical system. On the other hand, the proposed detector is robust against residual phase error and residual frequency offset. The proposed detector achieves SNR = −1.3 dB at the sensitivity level with or without impairments. The performance of the proposed detector is 3.8 dB better than that of the coherent detector when residual phase error and residual frequency offset remain. The differential detector in Yin et al. [18] and the conventional MSK differential detector are not sensitive to either. The differential detector in Yin et al. [18] achieves the sensitivity at SNR = 2.9 dB. The performance of the proposed detector is 4.2 dB better than that of differential detector in Yin et al. [18]. The conventional MSK differential detector, which has the least computational complexity among these detectors, achieves the sensitivity at SNR = 8.4 dB. The performance of the conventional MSK differential detector is significantly worse than any other detectors.

In the second simulation, we explore the performance of demodulators in the design of real systems shown in Fig. 9. The initial phase mismatch is uniformly distributed in

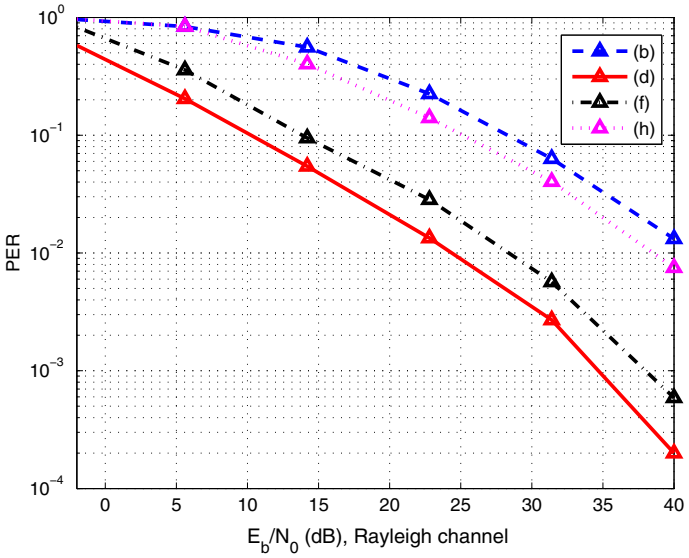

Fig. 10 Performance of demodulators in Rayleigh flat-fading channel. The initial phase mismatch is uniformly distributed in $[-\pi, \pi)$, and the frequency offset is uniformly distributed in [−200 kHz, 200 kHz). The initial phase mismatch is estimated and compensated in timing sync block. The frequency offset is estimated with the SKD estimator in frequency offset estimator block. *Lines* (*b*), (*d*), (*f*) and (*h*) show the PER performance of a demodulation system with initial phase mismatch and frequency offset of the coherent detector, the proposed detector, the differential detector in Yin et al. [18] and the conventional MSK differential detector, respectively

$[-\pi, \pi)$, and the frequency offset is uniformly distributed in [−200 kHz, 200 kHz). The initial phase mismatch is estimated and compensated in timing sync block. The frequency offset is estimated with the SKD estimator in frequency offset estimator block. Residual phase error and frequency offset still remain due to imperfection of the estimation. Similar to the first simulation, Lines (b), (d), (f) and (h) show the PER performance of a demodulation system with initial phase mismatch and frequency offset of the coherent detector, the proposed detector, the differential detector in Yin et al. [18] and the conventional MSK differential detector, respectively. At the sensitivity level, the performance of the proposed detector, the differential detector in Yin et al. [18] and the conventional MSK detector keeps the same at SNR = −1.3 dB, SNR = 2.9 dB and SNR = 8.4 dB, respectively. However, the performance of the coherent demodulator with frequency offset degrades remarkably. Further analysis shows that the SKD estimation results in a larger variance of residual frequency offset than the CRLB, which is the key contributor to the degradation of the coherent demodulator performance. The performance of the proposed demodulator is 4.2 dB better than that of differential detector in Yin et al. [18] and 9.7 dB better than that of conventional MSK differential demodulator in the design of real systems.

To show the improvement and effectiveness of the proposed demodulator, we inserted a third simulation with the same settings as the second simulation except that Rayleigh flat-fading channel is utilized. In Fig. 10, lines (b), (d), (f) and (h) show

the PER performance of a demodulation system with initial phase mismatch and frequency offset of the coherent detector, the proposed detector, the differential detector in Yin et al. [18] and the conventional MSK differential detector, respectively. At the sensitivity level, the required SNRs are 42, 24, 28 and 38 dB for the coherent detector, the proposed detector, the differential detector in Yin et al. [18] and the conventional MSK differential detector, respectively. The proposed demodulator outperforms other demodulators in the fading channel as well.

6 Conclusion

In this paper, we propose a robust non-coherent demodulator for OQPSK–DSSS system. The proposed demodulator achieves near optimal performance and is robust against initial phase mismatch and frequency offset. At the sensitivity level, the required SNR of the proposed demodulator with initial phase mismatch and frequency offset is -1.3 dB in AWGN channel and 24 dB in Rayleigh flat-fading channel at PER $= 1\,\%$. In comparison with other demodulators, more than 4 dB performance gain is achieved. In addition, the computational overhead of the proposed demodulator is similar to that of coherent demodulator or other differential non-coherent demodulators.

Acknowledgments This work was supported in part by the 100 Talents Program of Chinese Academy of Sciences, the National Natural Science Foundation of China (No. 61231009), and the Innovation Foundation of Shanghai Science and Technology (No. 11DZ1500201).

References

1. R. Chen, H. Huang, M. Hsieh, Design of an improved CMOS phase/frequency detector. Circuits Syst. Signal Process. **25**(4), 539–557 (2006)
2. S. Fang, S. Berber, A. Swain, S. Rehman, A study on DSSS transceivers using OQPSK modulation by IEEE 802.15.4 in AWGN and flat Rayleigh fading channels, in *Proceedings of IEEE Region 10 Conference on TENCON*, pp. 1347–1351 (2010)
3. A. Ghazi, J. Boutellier, J. Hannuksela, Low-complexity SDR implementation of IEEE 802.15.4 (ZigBee) baseband transceiver on application specific processor, in *Proceedings of Wireless Innovation Forum Conference on Wireless Communications Technologies and Software Defined Radio* (2013)
4. IEEE Std 802.15.4-2006, *IEEE Standard for Information Technology Part 15.4: Wireless Medium Access Control (MAC) and Physical Layer (PHY) Specifications for Low-Rate Wireless Personal Area Networks (WPANs)* (2006)
5. D. Kreiser, S. Olonbayar, Improvements of IEEE 802.15. 4a for non-coherent energy detection receiver Signals, in *Proceedings of IEEE International Symposium on Systems, and Electronics*, pp. 1–5 (2012)
6. S. Kay, A fast and accurate single frequency estimator. IEEE Trans. Acoust. Speech Signal Process. **37**(12), 1987–1990 (1989)
7. J. Lee, Performance evaluation of IEEE 802.15.4 for low-rate wireless personal area networks. IEEE Trans. Consum. Electron. **52**(3), 742–749 (2006)
8. S. Lanzisera, K. Pister, Theoretical and practical limits to sensitivity in IEEE 802.15.4 receivers, in *Proceedings of IEEE International Conference on Electronics, Circuits and Systems (ICECS'2007)*, pp. 1344–1347 (2007)
9. R. McKilliam, B. Quinn, I. Clarkson, B. Moran, Frequency estimation by phase unwrapping. IEEE Trans. Signal Process. **58**(6), 2953–2963 (2010)
10. H. Meyr, M. Moeneclaey, *Digital Communication Receivers: Synchronization, Channel Estimation and Signal Processing* (Wiley, New York, 1998), pp. 455–504

11. F. Olver, D. Lozier, *NIST Handbook of Mathematical Functions, Chapter 10*. (Cambridge University Press, Cambridge, 2010)
12. D. Park, C. Park, K. Lee, Simple design of detector in the presence of frequency offset for IEEE 802.15.4 LR-WPANs. IEEE Trans. Circuits Syst. **56**(4), 330–333 (2009)
13. S. Park, D. Park, Low-complexity frequency-offset insensitive detection for orthogonal modulation. Electron. Lett. **41**, 1226–1228 (2005)
14. D. Rife, R. Boorstyn, Single-tone parameter estimation from discrete-time observations. IEEE Trans. Inf. Theory **20**(5), 591–598 (1974)
15. C. Wang, J. Huang, A low-Power 2.45 GHz ZigBee transceiver for wearable personal medical devices in WPAN, in *Proc. IEEE International Conference on Consumer Electronics (ICCE'2007)*, pp. 1–2 (2007)
16. C. Wang, G. Sung, J. Huang, L. Lee, C. Li, A low-power 2.45 GHz WPAN modulator/demodulator. Microelectron. J. **41**(2), 150–154 (2010)
17. Y. Yu, X. Meng, S. Xiao, C. Ma, T. Ye, A new low-cost demodulator for 2.4 GHz ZigBee receivers. J. Electron. (China) **26**(2), 252–257 (2009)
18. S. Yin, J. Cui, A. Luo, L. Liu, S. Wei, A high efficient baseband transceiver for IEEE 802.15.4 LR-WPAN systems, in *Proceedings IEEE 9th International Conference on ASIC*, pp. 224–227 (2011)